

Impact of Joule heating and multiple slips on a Maxwell nanofluid flow past a slendering surface

Shafiq Ahmad^{1,*}, Muhammad Naveed Khan¹, Sohail Nadeem¹,
Aysha Rehman², Hijaz Ahmad³ and Rifaqat Ali⁴

¹Department of Mathematics, Quaid-I-Azam University 45320, Islamabad 44000, Pakistan

²Department of Mathematics, University of Gujrat, Gujrat, 50700 Pakistan

³Section of Mathematics, International Telematic University Uninettuno, Corso Vittorio Emanuele II, 39;00186 Roma, Italy

⁴Department of Mathematics, College of Science and Arts, Muhayil, King Khalid University 9004, Abha, Saudi Arabia

E-mail: ashafiq@math.qau.edu.pk

Received 12 June 2021, revised 18 October 2021

Accepted for publication 22 November 2021

Published 21 December 2021



Abstract

This manuscript presents a study of three-dimensional magnetohydrodynamic Maxwell nanofluid flow across a slendering stretched surface with Joule heating. The impact of binary chemical reactions, heat generation, thermal radiation, and thermophoretic effect is also taken into consideration. The multiple slip boundary conditions are utilized at the boundary of the surface. The appropriate similarity variable is used to transfer the flow modeled equations into ODEs, which are numerically solved by the utilization of the MATLAB bvp4c algorithm. The involved parameter's impact on the concentration, velocity, and temperature distribution are scrutinized with graphs. The transport rates (mass, heat) are also investigated using the same variables, with the results reported in tabulated form. It is seen that the fluid relaxation, magnetic, and wall thickness characteristics diminish the velocities of fluid. Further, the velocity, concentration, and temperature slip parameters reduce the velocities of fluid, temperature, and concentration distribution. The results are compared to existing studies and shown to be in dependable agreement.

Keywords: Maxwell nanofluid, slendering stretching surface, Joule heating, thermal radiation, thermophoretic effect

(Some figures may appear in colour only in the online journal)

1. Introduction

The heat and flow transport scrutiny on stretchable surfaces has a remarkable engineering application such as improvement in the efficiency of paints and lubrication, manufacturing of glass fiber, paper production, glass blowing, aerodynamic extrusion of rubber sheets, and crystal growing, etc. Many researchers have discussed the flow over a stretchable/non-stretchable and linear/nonlinear surface.

However, from the applicable point of view in real life, a stretching sheet of variable thickness can be more promising and effective in practical applications in plastic film, metal sparing, polymer extrusion, metallurgical process, etc. The flow over a variable thickness surface (slendering surface) has been given little attention. Although, some literature can be found related to the variable thickness surfaces. Nagen-dramma *et al* [1] discussed the 3D Casson nanofluid flow past a slendering surface in the presence of Cattaneo–Christov heat flux and slip effects. They found that velocity gradient is highly motivated due to increase in velocity slip parameter.

* Author to whom any correspondence should be addressed.

Prakash and Devi [2] employed a hydromagnetic hybrid nanofluid flow to improve heat transfer rate across a slendering sheet at a prescribed surface temperature. It is also observed that hybrid nanofluid exceeds nanofluid in terms of efficiency. The magnetohydrodynamic (MHD) stagnation point flow of third grade fluid towards a slendering stretching surface in the involvement of variable thermal conductivity and double stratification effects is examined by Hayat *et al* [3]. It is determined that increasing the magnetic parameter reduces the velocity field, whereas the wall thickness variable has the opposite effect. Reddy *et al* [4] characterized the nanofluid flow with MHD in the existence of slip effects through a slendering extending surface. Thermophoresis and Brownian parameters were shown to be capable of inflating the fluid temperature. Gayatri *et al* [5] demonstrated numerically the features of the nonlinear convective flow of Maxwell fluid along with the heat source/sink past a slendering stretching surface. They noticed that when a melting surface is present, the rate of heat transfer is much higher than when it is not. This result leads us to the conclusion that the melting surface is suitable for heating treatment. Reddy *et al* [6] emphasized the influence of activation energy and thermal nonlinear radiation on an MHD Eyring–Powell flow of nanofluid induced by slendering stretching surface. It is worth noting that larger values of radiative heat transport have a greater impact on temperature. In the presence of magnetohydrodynamic and thermal radiation, Mabood *et al* [7] investigate the boundary layer analysis of two-dimensional unsteady hybrid nanofluid flow across a flat/slendering stretched surface. The study's main finding is that increasing the magnetic field and nanoparticle volume fraction parameters reduces skin friction while increasing the rate of heat transfer. Kumar *et al* [8] evaluated the flow and heat-transfer characteristics of hybrid ferrofluid caused by the stretching of an unsteady surface under the effect of an irregular heat source/sink. Simultaneous solutions for ferrofluids and hybrid ferrofluids are offered. Recently, Kumar *et al* [9] want to look at the flow and heat transfer characteristics of a time-independent stagnation point flow of an electrically conducting magnetohydrodynamic micropolar fluid across a variable thickness surface. Some latest literature related to variable thickness sheets is presented in the [10, 11].

The quality of the product in the extrusion process mainly depends upon the mechanism of mass and heat transport. The transport of mass and heat has widespread applications in engineering and industrial processes. Some applications can be mentioned here, such as energy production, cooling reactor, power generation, and many more. The transport of mass and heat are used in controlling pollution and food industries. Mass diffusion by Fick's law and thermal conduction by Fourier's law can characterize the mechanism of mass and heat transport. Iqbal *et al* [12] examined the elements of thermal and solutal energy transfer in MHD Burger's nanofluid dynamics. They used Fourier's and Fick's laws to investigate heat and mass transfer processes. Heat transfer analysis of Cu–Al₂O₃ hybrid nanofluid with heat flow and viscous dissipation was performed by Ali *et al* [13]. When heat and mass transport phenomena are combined with other important features such as internal heat

generation and absorption, thermal diffusion effects, thermal radiations, nanofluidics, diffusion thermo effects, and variable transport properties, the analysis for three-dimensional flow past a stretching surface is more declines. In the presence of homogeneous-heterogeneous chemical reactions and entropy formation, Khan *et al* [14] studied the heat and mass transfer flow of a hybrid nanofluid including Hall and ion-slip effects. Sheikholeslami *et al* [15] use an experimental approach to show the results for nano-refrigerant boiling thermal transport within straighten channels. The findings show that raising the flattened fraction improves heat transfer. Furthermore, increasing the concentration of nanoparticles increases heat transfer within the ranges of the current experiment. Kumar [16] discussed the properties of heat transport and non-Newtonian nanofluid flow above an extending sheet with chemical reaction and factor of slip. The transport of heat and mass transfer of an unsteady 3D MHD flow of Maxwell nanofluid with temperature dependent transport properties, Joule heating, and chemical reaction is explored by Ahmad *et al* [17]. They found that as the Deborah number increases, the velocity of the fluid decreases because it provides resistance to fluid motion. Kumar *et al* [18] introduced the heat transport and flow of non-Newtonian fluids numerically, by considering the Darcy–Forchheimer and convective boundary conditions. The factor of slip lowers the field of velocity, while the Biot number raises the distribution of heat. Malik *et al* [19] described the features of mass and heat transfer on Sisko fluid by the consequence of Cattaneo–Christov theory along with an extending cylinder. Heat transport exploration across a curved stretched surface in the presence of uniform magnetohydrodynamics is described numerically by Ahmad *et al* [20]. Awais *et al* [21] observed the transportation of mass and heat transport on Casson MHD fluid flowing across a medium porous with the shrinking wall. Experimental investigation of thermal transport across oscillating flow inside a cylindrical tube is described by Bouvier *et al* [22]. The observation of mass and heat transport on nanomaterial non-Newtonian liquid flow induced by chemical reaction and activation energy is deliberated by Punith Gowda *et al* [23]. Considering different alternating magnetic fields, Zhang, and Zhang [24] investigated the heat transfer and pressure drop performance of magnetic nanofluids. The results demonstrated that alternating magnetic fields had a better effect on local heat transfer coefficients than unidirectional and non-magnetic fields in the same flow direction. Recently many latest studies related to heat, mass, and flow transfer are presented in the [25–28].

Slip conditions appear in the fluid where the viscous effects at the wall are negligible. Slip conditions are very necessary for many situations, like lubricated hydrophobic surfaces, porous and rough surfaces, coated surfaces, microvalve, micro nozzle, micro pumps, etc. On the other hand, nanoparticles and non-Newtonian fluids are not occupied the no-slip boundary conditions. Navier [29] first time developed the velocity slip boundary conditions followed by Maxwell [30]. Andersson [31] evaluated the slip Newtonian liquid flow through an extending surface. Nawaz *et al* [32] investigated the effects of chemical reaction, partial slip, thermal temperature, and concentration slip on mass and heat transfer in a liquid with variable thermophysical parameters numerically. They determined that the

diffusion of wall momentum in a fluid with constant viscosity is faster than the diffusion of wall momentum in a fluid with variable viscosity as temperature rises. In the influence of slip condition and thermophoretic mechanisms, Archana *et al* [33] examine the incompressible and squeezed Casson nanofluid flow between two parallel plates. The velocity component is found to be increased for the bigger squeezed parameter and slip parameter, although the temperature component follows the same pattern for Brownian motion and thermophoresis. Imran *et al* [34] anticipated the natural convection and radiative Maxwell liquid flow towards an exponentially extending surface along with slip conditions. The transfer of heat and flow investigation on MHD Maxwell nanofluid under the impact of variable thermal conductivity and slip conditions is carried out by Aziz and Shams [35]. As a result of thermal radiation and the slip effect, Souayah *et al* [36] study a mathematical model for heat transport and dusty hybrid flow of nanofluid on a stretched surface. They noticed that higher Pr values indicate a decline in heat transfer for both phases. Furthermore, when compared to ordinary nanofluid flow, hybrid nanomaterial flow performs a more effective function in the heat transportation process. The transport of heat and flow on a hybrid nanomaterial liquid with entropy generation and slip boundary conditions across an extending nonlinear surface was studied by Ahmad *et al* [37]. Khan and Alzahrani [38] observed the Jeffrey nanofluid flow with combined features of Joule heating, slip effects, activation energy, magnetohydrodynamics (MHD), and thermophoresis diffusion. Above a nonlinear stretching sheet, Ahmad and Nadeem [39] numerically investigated the 3D radiative hybrid nanofluid flow in the presence of mixed convection, Darcy–Forchheimer, nonlinear source/sink, and activation energy. They showed that when the solid volume concentration of hybrid nanofluid is added, the heat transfer rate is high. Recently some researchers discuss the characteristics of mass and heat transport with slip effects and Joule heating (see [40–42]).

Furthermore, one of the most dominant variables in thermal transport processes is Joule heating. When a flow is transported via a magnetic field, the temperature of the fluid rises. This type of phenomenon arises when atomic molecules interact with moving molecules. Electric heaters, incandescent light bulbs, cartridge heaters, electric stoves, soldering irons, food processing, electric fuses, vegetable glycerine, electronic cigarettes, thermistor, and other industrial and technological applications employ joule heating. In light of certain implications, Swain *et al* [43] inspected the role of Joule heating and viscous dissipation on Williamson hydromagnetic liquid flow towards a nonlinear extending sheet embedded in a porous medium. With the influence of the magnetic field, Joule heating, and the Soret effect, Palaiah *et al* [44] evaluate the mass and heat transport features of Maxwell two-dimensional steady fluid flow via an extending surface. They determined that as the magnetic parameter was increased, the normal and axial velocity profiles decreased. The temperature and concentration profiles in the flow zone are reduced by increasing the Prandtl and Schmidt numbers, respectively. Ahmed *et al* [45] explore the solutal energy and thermal transport in the nano-Maxwell liquid flow across a porous medium with Joule heating, heat generation, and chemical reaction effects. Abdelhafez *et al* [10] describe an unsettled

2D influx of Maxwell nanofluid induced by an extending cylinder embedded in a porous medium with the impact of Joule heating and chemical reaction. They found that the Biot number and order of chemical reactions improves the rate of heat transfer. Islam *et al* [46] evaluate the thermal effects of a Maxwell mixed convection nanofluid flow spinning motion generated by a bidirectional and rotating stretching cylinder, taking into account the effects of an internal heat source/sink and Joule heating.

In the aforementioned literature, no study has been done yet to investigate the features of transfer of mass and heat on 3D Maxwell nanofluid flow across a slendering stretching sheet under the thermophoretic and radiation effects. Further, the multiple slip boundary conditions are implemented on the boundary of the surface. The obtained differential equations are turned into coupled ODEs by the utilization of relevant similarity variables. The solutions algorithm Bvp4c is used to manipulate the coupled ODEs. The outcomes are obtained and conferred by the assistance of graphs. The numerical values for mass and heat transport rate are presented in the table for different parameters. The following is the layout of this article: section one—introduction. The second section is dedicated to mathematical modeling, which includes all necessary equations as well as the application of boundary layer theory to partial differential equations. The results and discussion are covered in the third section. The paper comes to a close with some closing remarks and a summary.

2. Mathematical modeling

Consider, 3D, incompressible, laminar, electrically conducting Maxwell flow of nanofluid across a stretching surface of variable thickness with bearing slip effects. Effects of magneto hydrodynamics (MHD), viscous dissipation, heat generation, Joule heating, binary chemical reaction, and thermophoretic effect are also considered. The $z = J(c + x + y)^{\frac{(1-n)}{2}}$ can be considered as the variable thickness of the sheet. To make the sheet sufficiently thin, we choose J small, we also assumed that the stretching velocities in x - and y -directions are $\bar{u}_w = a(c + x + y)^{\frac{(1-n)}{2}}$ and $\bar{v}_w = b(c + x + y)^{\frac{(1-n)}{2}}$ respectively. Here n is the power-law index and it consider $n \neq 0$, because for $n = 1$ results to a flat surface, also for $n < 1$ and $n > 1$ are the surface shapes yields to inner convex and outer convex by the reduction and augmentation of wall thickness respectively. The flow region is $z \geq 0$, in which z -axis is normal to xy -plane. Figure 1 shows a representation of the physical model. In the direction normal to the sheet, a non-uniform magnetic field $B(x, y)$ is applied. The concentration and temperature at the boundary of the surface are represented by \bar{C}_w and \bar{T}_w respectively, and away from the surface, it signifies by \bar{C}_∞ and \bar{T}_∞ respectively.

By the utilization of the above supposition, the developed equations are in the form,

$$\nabla \cdot \mathbf{V} = 0, \quad (1)$$

$$\rho(\mathbf{V} \cdot \nabla)\mathbf{V} = \nabla \cdot \mathbf{S} - \nabla \cdot \mathbf{P} + \rho\mathbf{E} + \mathbf{J} \times \mathbf{B}, \quad (2)$$

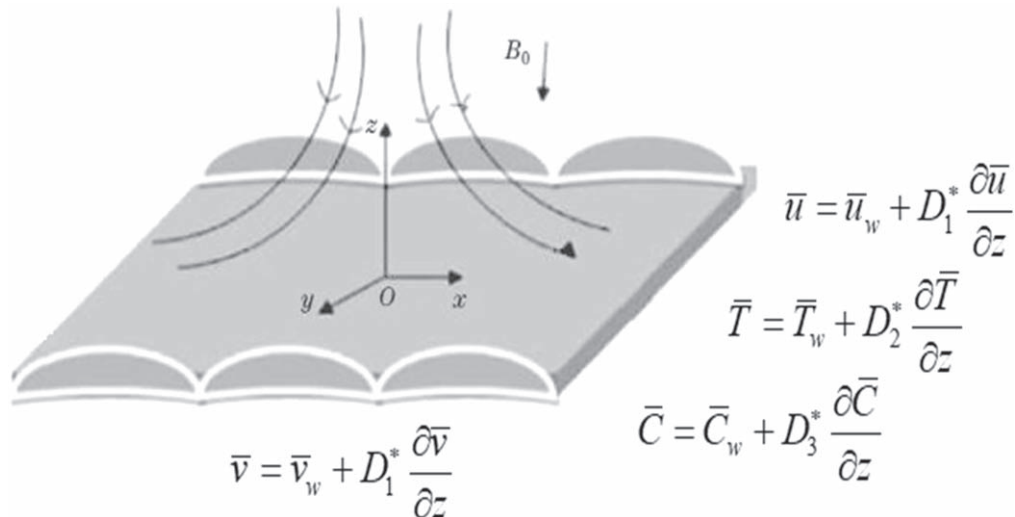


Figure 1. Flow configuration of the problem.

$$\rho c_p [\mathbf{V} \cdot \nabla \bar{T}] = \alpha \nabla^2 \bar{T} + \frac{\tau D_{\bar{T}}}{\bar{T}_{\infty}} (\nabla \bar{T})^2 - Q_r + Q_0, \quad (3)$$

$$[\mathbf{V} \cdot \nabla \bar{C}] = D_B \nabla^2 \bar{C} + \frac{D_{\bar{T}}}{\bar{T}_{\infty}} \nabla^2 \bar{T} - V_{\bar{T}}. \quad (4)$$

Here ρ is the density of the fluid, D_B is the mass diffusivity, α is the thermal diffusivity, $\rho \mathbf{E} + \mathbf{J} \times \mathbf{B}$ is the body forces, Q_r is the radiative heat flux, Q_0 is the heat generation/absorption, τ is the ratio of capacities (molecular to heat), $V_{\bar{T}}$ is the thermophoretic velocity effect, c_p is specific heat. The extra stress tensor for Maxwell fluid is \mathbf{S} , which is defined as,

$$\left(1 + \lambda_0 \frac{D}{Dt}\right) \mathbf{S} = \mu \mathbf{A}_1, \quad (5)$$

where \mathbf{A}_1 is the Rivlin–Ericksen tensor ($\mathbf{A}_1 = (\nabla \mathbf{V})^t + \nabla \mathbf{V}$), λ_0 is the relaxation time, μ is the viscosity, and $\frac{D}{Dt}$ is the material derivative. Invoking the boundary layer approximation, the above equations become [40, 42],

$$\frac{\partial \bar{u}}{\partial x} = -\left(\frac{\partial \bar{w}}{\partial z} + \frac{\partial \bar{v}}{\partial y}\right), \quad (6)$$

$$\begin{aligned} & \bar{u} \frac{\partial \bar{u}}{\partial x} + \bar{v} \frac{\partial \bar{u}}{\partial y} + \bar{w} \frac{\partial \bar{u}}{\partial z} \\ & + \lambda_0 \left[\bar{u} \left(\frac{\partial^2 \bar{u}}{\partial x^2} + 2\bar{v} \frac{\partial^2 \bar{u}}{\partial x \partial y} \right) + \bar{v}^2 \frac{\partial^2 \bar{u}}{\partial y^2} \right. \\ & \left. + 2\bar{w} \left(\bar{v} \frac{\partial^2 \bar{u}}{\partial y \partial z} + \bar{u} \frac{\partial^2 \bar{u}}{\partial x \partial z} \right) + \bar{w}^2 \frac{\partial^2 \bar{u}}{\partial z^2} \right] \\ & = \nu \frac{\partial^2 \bar{u}}{\partial z^2} - \frac{\sigma B^2}{\rho} \left(\bar{u} + \lambda_0 \bar{w} \frac{\partial \bar{u}}{\partial z} \right), \end{aligned} \quad (7)$$

$$\begin{aligned} & \bar{u} \frac{\partial \bar{v}}{\partial x} + \bar{v} \frac{\partial \bar{v}}{\partial y} + \bar{w} \frac{\partial \bar{v}}{\partial z} \\ & + \lambda_0 \left[\bar{u} \left(\frac{\partial^2 \bar{v}}{\partial x^2} + 2\bar{v} \frac{\partial^2 \bar{v}}{\partial x \partial y} \right) + \bar{v}^2 \frac{\partial^2 \bar{v}}{\partial y^2} \right. \\ & \left. + 2\bar{w} \left(\bar{v} \frac{\partial^2 \bar{v}}{\partial y \partial z} + \bar{u} \frac{\partial^2 \bar{v}}{\partial x \partial z} \right) + \bar{w}^2 \frac{\partial^2 \bar{v}}{\partial z^2} \right] \\ & = \nu \frac{\partial^2 \bar{v}}{\partial z^2} - \frac{\sigma B^2}{\rho} \left(\bar{v} + \lambda_0 \bar{w} \frac{\partial \bar{v}}{\partial z} \right), \end{aligned} \quad (8)$$

$$\begin{aligned} & \bar{u} \frac{\partial \bar{T}}{\partial x} + \bar{v} \frac{\partial \bar{T}}{\partial y} + \bar{w} \frac{\partial \bar{T}}{\partial z} = \tau D_B \frac{\partial \bar{T}}{\partial z} \frac{\partial \bar{C}}{\partial z} \\ & + \alpha \frac{\partial^2 \bar{T}}{\partial z^2} + \frac{1}{\rho c_p} \left(Q_0 (\bar{T}_w - \bar{T}_{\infty}) - \frac{\partial Q_r}{\partial z} \right) \\ & + \frac{\tau D_{\bar{T}}}{\bar{T}_{\infty}} \left(\frac{\partial \bar{T}}{\partial z} \right)^2, \end{aligned} \quad (9)$$

$$\begin{aligned} & \bar{u} \frac{\partial \bar{C}}{\partial x} + \bar{v} \frac{\partial \bar{C}}{\partial y} + \bar{w} \frac{\partial \bar{C}}{\partial z} = D_B \frac{\partial^2 \bar{C}}{\partial z^2} \\ & - \left(\frac{\partial}{\partial z} (V_{\bar{T}} \bar{C}) + \Gamma_0 (\bar{C}_w - \bar{C}_{\infty}) \right) \\ & + \frac{D_{\bar{T}}}{\bar{T}_{\infty}} \frac{\partial^2 \bar{T}}{\partial z^2}. \end{aligned} \quad (10)$$

The suitable boundary conditions are defined as [40],

$$\begin{aligned} & \left(\bar{u} = \bar{u}_w + D_1^* \frac{\partial \bar{u}}{\partial z}, \quad \bar{v} = \bar{v}_w + D_1^* \frac{\partial \bar{v}}{\partial z}, \quad \bar{w} = 0, \right. \\ & \left. \bar{T} = \bar{T}_w + D_2^* \frac{\partial \bar{T}}{\partial z}, \quad \bar{C} = \bar{C}_w + D_3^* \frac{\partial \bar{C}}{\partial z} \right) \\ & \text{at } z = J(c + x + y)^{\frac{1-n}{2}}. \end{aligned} \quad (11)$$

$$\begin{aligned} & \bar{u} \rightarrow 0, \quad \bar{v} \rightarrow 0, \quad \bar{T} \rightarrow \bar{T}_{\infty}, \quad \bar{C} \rightarrow \bar{C}_{\infty}, \\ & \text{at } z \rightarrow \infty. \end{aligned} \quad (12)$$

Where,

$$Q_r = -\frac{4\sigma^*}{3k_l} \frac{\partial \bar{T}^4}{\partial z}, \quad V_{\bar{T}} = -\nu \frac{k_r^*}{\bar{T}_r} \frac{\partial \bar{T}}{\partial z}. \quad (13)$$

$$\begin{aligned} \bar{u}_w &= a(c+x+y)^{\frac{(1-n)}{2}}, \quad \Gamma = \Gamma_0(c+x+y)^{n-1}, \\ \bar{T}_w &= \bar{T}_\infty + \bar{T}_0(c+x+y)^{\frac{(1-n)}{2}}, \quad Q = Q_0(c+x+y)^{n-1}, \\ \bar{v}_w &= b(c+x+y)^{\frac{(1-n)}{2}}, \quad \bar{C}_w = \bar{C}_\infty + \bar{C}_0(c+x+y)^{\frac{(1-n)}{2}}, \\ B &= B_0(c+x+y)^{\frac{(1-n)}{2}}. \end{aligned} \quad (14)$$

In equation (13), we expand \bar{T}^4 by utilization of the Taylors series about \bar{T}_∞ and ignoring higher-order terms in the form $\bar{T}^4 \cong 4\bar{T}_\infty^3 \bar{T} - 3\bar{T}_\infty^4$.

In above equations (6)–(14) the symbols λ_0 , σ , ρ , ν , $D_{\bar{T}}$, Γ_0 , σ^* , k_l , νk_r^* and \bar{T}_r are represented the fluid relaxation time, electrical conductivity, fluid density, kinematics viscosity, coefficient Brownian motion, coefficient thermophoresis, chemical reaction constant, Stefan–Boltzmann constant, coefficient mean absorption, thermophoretic coefficient, and reference temperature respectively.

2.1. Similarity transformation

The relevant similarity variables are characterized as [6, 40],

$$\begin{aligned} \bar{u} &= a(c+x+y)^n F'(\xi), \quad \xi = z \sqrt{\frac{a(n+1)}{2\nu}} (c+x+y)^{\frac{(n-1)}{2}}, \\ \bar{v} &= a(c+x+y)^n G'(\xi), \\ w &= -\left(\frac{2a\nu}{n+1}\right)^{\frac{1}{2}} (c+x+y)^{\frac{n-1}{2}} \left((n+1) \left(\frac{F(\xi) + G(\xi)}{2} \right) \right. \\ &\quad \left. + (n-1) \xi \left(\frac{F'(\xi) + G'(\xi)}{2} \right) \right), \\ \bar{T} - \bar{T}_\infty &= (\bar{T}_w - \bar{T}_\infty) \Theta(\xi), \quad \bar{C} - \bar{C}_\infty = (\bar{C}_w - \bar{C}_\infty) \Phi(\xi). \end{aligned} \quad (15)$$

Using equation (15) the dimensionless form of equations (6)–(12) is,

$$\begin{aligned} (n+1) \left(\frac{F'''}{2} + \left(\frac{F+G}{2} \right) F'' \right) &+ M\beta \left\{ (n+1) \left(\frac{F+G}{2} \right) \right. \\ &\quad \left. + \xi(n-1) \left(\frac{F'+G'}{2} \right) \right\} F'' - MF' \\ &- \beta \left\{ 4n \left(\frac{n-1}{2} \right) (F'+G')^2 F' + 2\xi \left(\frac{n-1}{2} \right) \left(\frac{5n-7}{2} \right) (F'+G')^2 F'' \right. \\ &\quad \left. + \xi^2 \frac{(n-1)^2}{4} (F'+G')^2 F''' - (n+1)(F'+G')(F+G)F'' \right\} \\ &- 2n \left(\frac{F'+G'}{2} \right) F' = 0, \end{aligned} \quad (16)$$

$$\begin{aligned} (n+1) \left(\frac{G'''}{2} + \left(\frac{F+G}{2} \right) G'' \right) &+ M\beta \left\{ (n+1) \left(\frac{F+G}{2} \right) \right. \\ &\quad \left. + \xi(n-1) \left(\frac{F'+G'}{2} \right) \right\} G'' - MG' \\ &- \beta \left\{ 4n \left(\frac{n-1}{2} \right) (F'+G')^2 G' + 2\xi \left(\frac{n-1}{2} \right) \left(\frac{5n-7}{2} \right) (F'+G')^2 G'' \right. \\ &\quad \left. + \xi^2 \frac{(n-1)^2}{4} (F'+G')^2 G''' - (n+1)(F'+G')(F+G)G'' \right\} \\ &- 2n \left(\frac{F'+G'}{2} \right) G' = 0, \end{aligned} \quad (17)$$

$$\begin{aligned}
& \left(1 + \frac{4}{3}R_d\right)\Theta'' + Nb\Theta'\Phi' + Nt\Theta'^2 \\
& - \left(\frac{2Pr}{n+1}\right) \left[\left(\frac{1-n}{2}\right)(F' + G')\Theta - \left(\frac{n+1}{2}\right)(F + G)\Theta' \right] \\
& + Q\Theta + M(Ec_1F'^2 + Ec_2G'^2) \\
& = 0,
\end{aligned} \tag{18}$$

$$\begin{aligned}
& \Phi'' + \frac{Nt}{Nb}\Theta'' - Sc \left[\left(\frac{1-n}{n+1}\right)(F' + G')\Phi \right. \\
& \left. - (F + G)\Phi' - \delta(\Theta'\Phi' - (\Psi + \Phi)\Theta'') - \Gamma\Phi \right] = 0.
\end{aligned} \tag{19}$$

The convenient boundaries take the following form,

$$\begin{aligned}
& \left(\begin{aligned} F &= \alpha_1 \left(\frac{1-n}{1+n} \right) (1 + K_1 F''), \\ G &= \alpha_1 \left(\frac{1-n}{1+n} \right) (1 + K_1 G''), \quad F' = 1 + K_1 F'', \\ G' &= A + K_1 G'', \quad \Theta = 1 + K_2 \Theta', \quad \Phi = 1 + K_3 \Phi'. \end{aligned} \right) \\
& \text{at } \eta \rightarrow \alpha_1.
\end{aligned} \tag{20}$$

$$F' \rightarrow 0, \quad G' \rightarrow 0, \quad \Theta \rightarrow 0, \quad \Phi \rightarrow 0, \quad \text{at } \eta \rightarrow \infty. \tag{21}$$

To make computations easier, the interval $[\alpha_1, \infty)$ should be transformed $[0, \infty)$, we introduce the following functions,

$$\begin{aligned}
& \left(\begin{aligned} F(\xi) &= f(\zeta - \alpha_1) = f(\zeta), \\ G(\xi) &= g(\zeta - \alpha_1) = g(\zeta), \\ \Theta(\xi) &= \theta(\zeta - \alpha_1) = \theta(\zeta), \\ \Phi(\xi) &= \phi(\zeta - \alpha_1) = \phi(\zeta). \end{aligned} \right).
\end{aligned} \tag{22}$$

Using equation (22), the equations (16)–(21) takes the following forms,

$$\begin{aligned}
& (n+1) \left(\frac{f'''}{2} + \left(\frac{f+g}{2} \right) f'' \right) \\
& + M\beta \left\{ \left(\frac{n+1}{2} \right) (f+g) + \xi \left(\frac{n-1}{2} \right) (f' + g') \right\} f'' - Mf' \\
& - \beta \left\{ \begin{aligned} & 2n(n-1)(f' + g')^2 f' + \zeta(n-1) \left(\frac{5n-7}{2} \right) (f' + g')^2 f'' \\ & + \zeta^2 \left(\frac{n-1}{2} \right)^2 (f' + g')^2 f''' - (n+1)(f' + g')(f+g)f'' \end{aligned} \right\} \\
& - nf'(f' + g') = 0,
\end{aligned} \tag{23}$$

$$\begin{aligned}
& (n+1) \left(\frac{g'''}{2} + (f+g) \frac{g''}{2} \right) \\
& + M\beta \left\{ \left(\frac{n+1}{2} \right) (f+g) + \xi \left(\frac{n-1}{2} \right) (f' + g') \right\} g'' - Mg \\
& - \beta \left\{ \begin{aligned} & 2n(n-1)(f' + g')^2 g' + \zeta(n-1) \left(\frac{5n-7}{2} \right) (f' + g')^2 g'' \\ & + \zeta^2 \left(\frac{n-1}{2} \right)^2 (f' + g')^2 g''' - (n+1)(f' + g')(f+g)g'' \end{aligned} \right\} \\
& - ng'(f' + g') = 0,
\end{aligned} \tag{24}$$

$$\begin{aligned}
& \left(1 + \frac{4}{3}R_d\right)\theta'' + Nb\theta'\phi' + Nt\theta'^2 \\
& - \left(\frac{2Pr}{n+1}\right) \left[\left(\frac{1-n}{2}\right)(f' + g')\theta - \left(\frac{n+1}{2}\right)(f+g)\theta' \right] \\
& + Q\theta + M(Ec_1f'^2 + Ec_2g'^2) \\
& = 0,
\end{aligned} \tag{25}$$

$$\phi'' + \frac{N_t}{N_b}\theta'' - S_c \left[\left(\frac{1-n}{n+1} \right) (f' + g')\phi - (f + g)\phi' - \delta(\theta'\phi' - (\Psi + \phi)\theta'') - \Gamma\phi \right] = 0. \quad (26)$$

$$\left(\begin{array}{l} f = \alpha_1 \left(\frac{1-n}{1+n} \right) (1 + K_1 f''), \\ g = \alpha_1 \left(\frac{1-n}{1+n} \right) (1 + K_1 g''), \quad f' = 1 + K_1 f'', \\ g' = A + K_1 g'', \quad \theta = 1 + K_2 \theta', \quad \phi = 1 + K_3 \phi'. \end{array} \right) \quad (27)$$

at $\zeta \rightarrow 0$,

$$f' \rightarrow 0, \quad g' \rightarrow 0, \quad \theta \rightarrow 0, \quad \phi \rightarrow 0, \quad \text{at } \zeta \rightarrow \infty. \quad (28)$$

The evolving characteristics are fluid relaxation parameter, Eckert number in x -direction, magnetic parameter, radiation parameter, Eckert number y -direction, Brownian motion parameter, heat absorption/generation parameter, Prandtl number, concentration difference parameter, Schmidt number, thermophoresis parameter, temperature ratio parameter, stretching ratio parameter, and variable thickness parameter are symbolized by β , M , Ec_1 , R_d , Ec_2 , N_b , Q , Ψ , S_c , N_t , δ , Pr , A , and α_1 respectively. Further, K_1 , K_2 , and K_3 are the velocity slip, thermal jump, and concentration jump parameters, respectively. Mathematically these parameters are specified as,

$$\begin{aligned} Pr &= \frac{\nu}{\alpha}, \quad \delta = \frac{-k_r^*(\bar{T}_w - \bar{T}_\infty)}{\bar{T}_r}, \\ Q &= \frac{Q_0}{a\rho c_p}, \quad \beta = a\lambda_0, \quad S_c = \frac{\nu}{D_B}, \\ N_b &= \frac{\tau D_B \Delta \bar{C}}{\nu}, \\ \alpha_1 &= J \sqrt{\frac{a(n+1)}{2\nu}}, \quad R_d = \frac{4\sigma^* \bar{T}_\infty}{\kappa k_1}, \\ \Gamma &= \frac{\Gamma_0^2}{a}, \quad M = \sqrt{\frac{\sigma B_0^2}{a\rho}}, \quad N_t = \frac{\tau D_T \Delta \bar{T}}{\bar{T}_\infty \nu}, \quad A = \frac{b}{a}, \\ \Psi &= \frac{\bar{C}_w}{\bar{C}_w - \bar{C}_\infty}, \quad Ec_1 = \frac{u_w^2}{c_p(\bar{T}_w - \bar{T}_\infty)}, \\ Ec_2 &= \frac{v_w^2}{c_p(\bar{T}_w - \bar{T}_\infty)}. \end{aligned} \quad (29)$$

2.2. Physical quantities

The quantities concern to the physical point of view of the problem like Nusselt number and Sherwood are defined mathematically as,

$$Nu_x = \frac{xq_m}{\kappa(\bar{T}_w - \bar{T}_\infty)}, \quad Sh_x = \frac{xj_m}{D_B(\bar{C}_w - \bar{C}_\infty)}, \quad (30)$$

In equation (17) q_m is heat flux and j_m is mass flux, which is stated as,

$$q_m = - \left[\left(\kappa + \frac{16\sigma^* \bar{T}_\infty^3}{3k^*} \right) \frac{\partial \bar{T}}{\partial \zeta} \right]_{\zeta=0}, \quad j_m = -D_B \left[\frac{\partial \bar{C}}{\partial \zeta} \right]_{\zeta=0}. \quad (31)$$

The dimensionless form Nusselt and Sherwood number are defined as,

$$\begin{aligned} Nu_x(Re_x)^{-\frac{1}{2}} &= - \left(\frac{n+1}{2} \right)^{\frac{1}{2}} \left(1 + \frac{4}{3} R_d \right) \theta'(0), \\ Sh_x(Re_x)^{-\frac{1}{2}} &= - \left(\frac{n+1}{2} \right)^{\frac{1}{2}} \phi'(0). \end{aligned} \quad (32)$$

Table 1. Estimation of $f''(0)$ and $g''(0)$ with previous data, when $M = \alpha_1 = 0 = K_1 = K_2$.

n	A	Nandi <i>et al</i> [40]		Presents results	
		$f''(0)$	$g''(0)$	$f''(0)$	$g''(0)$
1.0	0.0	−1.000 007	0.000 00	−1.000 008	0.000 00
1.0	0.5	−1.224 76	−0.612 373	−1.224 78	−0.612 374
1.0	1.0	−1.414 422	−0.414 212	−1.414 424	−0.414 215
3.0	0.0	−1.624 357	0.000 00	−1.624 355	0.000 000
3.0	0.5	−1.989 423	−0.994 711	−1.989 425	−0.994 713
3.0	1.0	−2.229 7188	−2.297 188	−2.229 7186	−2.297 186

Table 2. Numerical values of $Re_x^{-1/2}Nu_x$ for several parameters.

R_d	n	Q	N_t	K_2	M	$Re_x^{-1/2}Nu_x$
0.1	0.3	1.0	0.1	0.5	0.1	0.795 52
0.3						0.880 35
0.5						0.938 24
	0.3					0.606 36
	0.4					0.634 21
	0.5					0.663 52
		0.2				0.434 22
		0.3				0.273 19
		0.4				0.226 14
			0.2			0.663 15
			0.3			0.608 27
			0.4			0.553 11
				0.2		0.407 81
				0.4		0.385 21
				0.6		0.360 43
					0.1	0.761 42
					0.3	0.702 80
					0.5	0.686 30

Table 3. Numerical values of $Re_x^{-1/2}Sh_x$ for several parameters.

N_b	n	S_c	δ	K_3	K_r	$Re_x^{-1/2}Sh_x$
0.2	0.3	3.0	1.0	0.5	1.0	0.411 74
0.4						0.455 79
0.8						0.496 71
	0.2					0.616 15
	0.4					0.617 19
	0.6					0.618 19
		2.0				0.461 96
		2.5				0.566 21
		2.9				0.589 19
			0.2			0.155 61
			0.3			0.425 01
			0.4			0.645 22
				1.0		0.546 21
				1.5		0.373 52
				2.0		0.247 71
					0.1	0.263 76
					0.3	0.465 22
					0.5	0.856 34

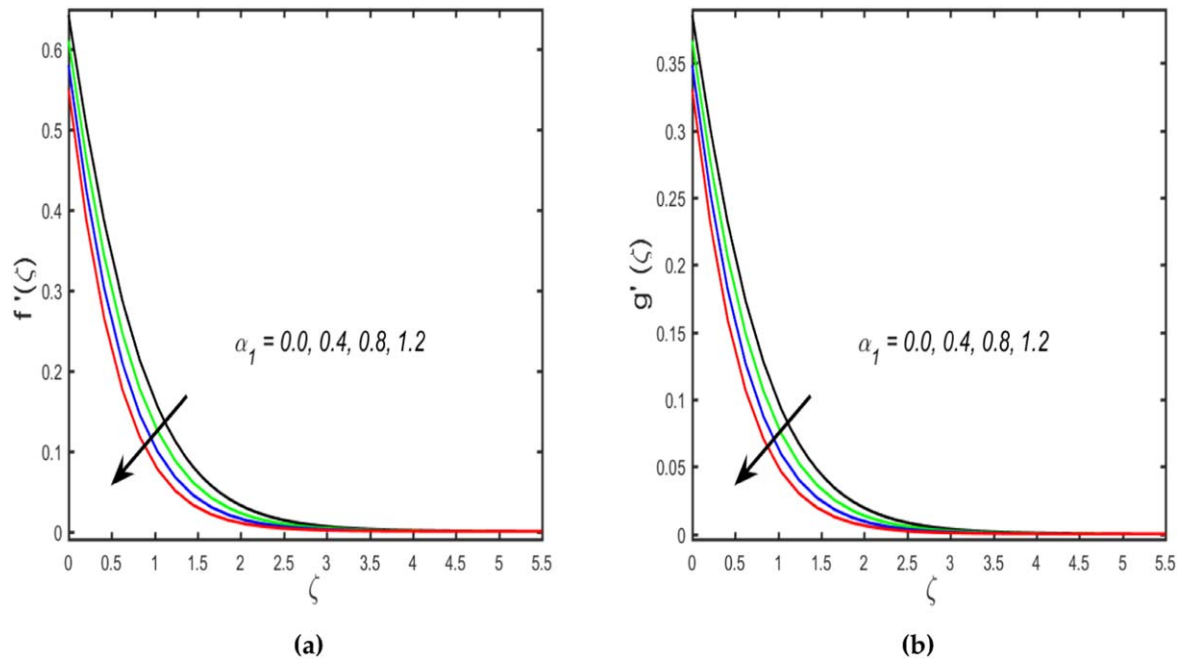


Figure 2. (a), (b): Variation in α_1 along $f'(\zeta)$ and $g'(\zeta)$ sketch.

$Re_x = \frac{(x+y+c)u_w}{\nu}$ is the Reynolds number.

3. Results and discussion

The three-dimensional Maxwell nanofluid flow by the impact of Joule heating, thermal radiation, multiple slips, and chemical reaction through a slendering stretching surface is observed in this study. In this section, we examine the physical configuration of various characteristics through the graph. The MATLAB bvp4c algorithm is utilized to solve the ordinary differential equation. Table 1 assesses the current problem classification to Nandi *et al* [40] available related results. This paper is in excellent alignment with a previously published study. Tables 2 and 3 described the numerical observation of Nusselt number and Sherwood number for several parameters. It is noted from the table 2, that the stronger values of n and R_d improve the heat transfer rate, while opposite trend is obtained for the growing values of Q , Nt , K_2 , and M declines the heat transfer rate. Further, table 3 observed that larger estimation of N_b , n , S_c , δ , and K_r boosts the mass transfer rate, whereas opposite trend is observed for the greater values of K_3 .

Figures 2(a) and (b) illustrates the consequences of α_1 (wall thickness characteristics) on the fluid velocities in the direction x - and y -axis. It is depicted from the figures that in both directions the velocity shows decreasing behavior by the larger estimation of wall thickness parameter. Physically, by increasing the α_1 retarding factor occurs which slowing down the velocity of fluid, as a result the momentum boundary layer thickness decreases. The influence of the β (fluid relaxation parameter) on the velocity field along the y - and x -axis direction is demonstrated in figures 3(a) and (b). The velocity sketch and thickness of the boundary layer are

designated to reduce as β increases. Physically, β is the relationship between observation and relaxation time; as relaxation time increases, resistance to liquid movement increases, resulting in reduction in the velocity $f'(\zeta)$ and $g'(\zeta)$. Moreover, due to increment of the β fluid behave like a solid and the fluidity of the fluid reduces, therefore fluid velocity declines consequently. The characteristic of Q (heat generation) on thermal distribution is observed in figure 4(a). The sketch clarify that the thermal sketch enlarges with the stronger estimation of Q . Physically, more heat is produced and the density of fluid reduces by the enlargement of Q , therefore the temperature and related boundary layer thickness boosts. The radiation parameter impact on the temperature sketch is scrutinized in figure 4(b). The thermal layer increases with larger estimation of R_d . Thermal radiation generates the extra heat energy in the fluid flow as this is the external source of energy which applied on surface of the geometry thus, the temperature distribution of flow increases. Figures 5(a)–(c) demonstrates the consequences of M (magnetic parameter) on fluid velocity and temperature field. The fluid velocities in x - and y -directions reduces by the increment of M . This is specified in figures 5(a) and (b). Further, fluid temperature increases due to larger estimation of M (see in figure 5(c)). The physics behind this is that the Lorentz force occurs with higher the magnetic parameter which produces resistance in the flow field, yields the fluid velocity contracts, and temperature enhances. The significance of velocity slip factor on the velocity distribution along x - and y -axis is demonstrated in figures 6(a) and (b). The figures show that $g'(\zeta)$ and $f'(\zeta)$ diminishes close to the boundary, although the opposite trend is shown afar from the solid boundary wall with the elevation of K_1 . This demonstrates that near the boundary wall, velocity slip tends to diminish velocities in both directions, however far away from

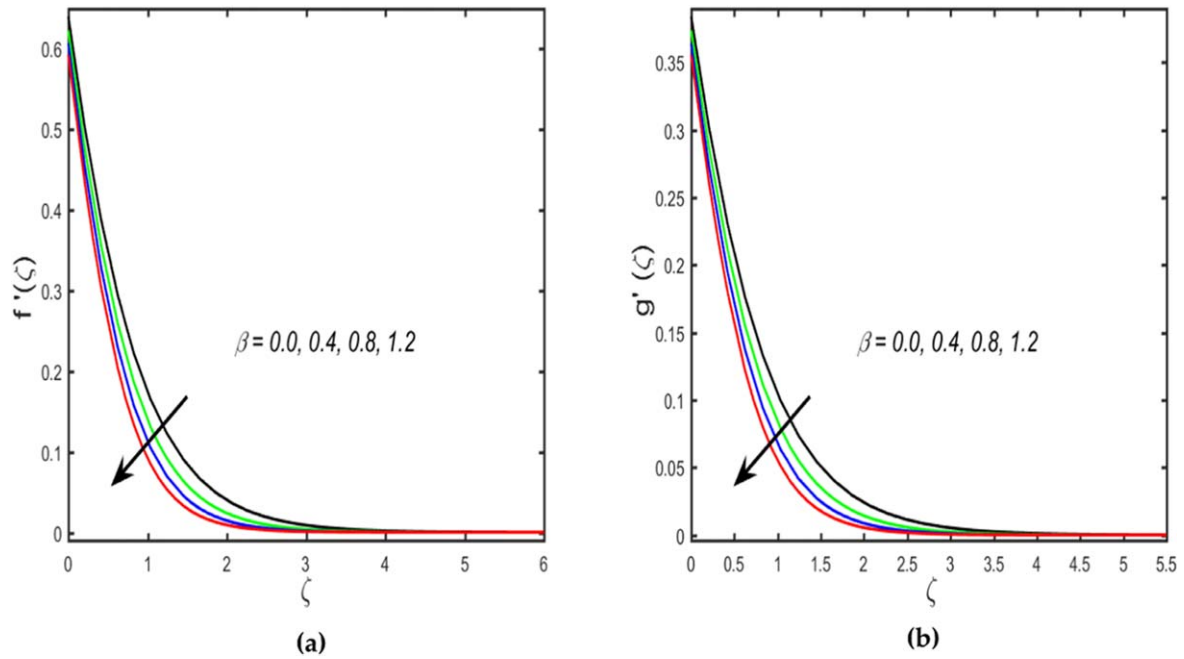


Figure 3. (a), (b): Variation in β along $f'(\zeta)$ and $g'(\zeta)$ sketch.

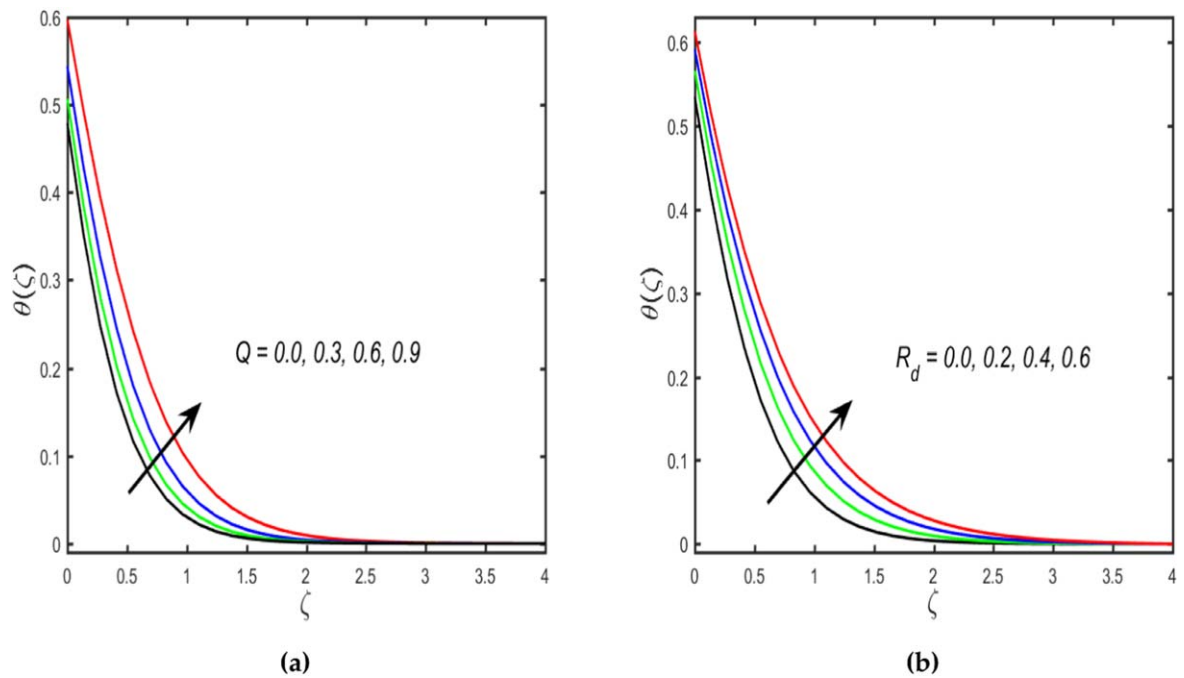


Figure 4. (a), (b): Plots of Q and R_d along $\theta(\zeta)$.

the boundary wall, they show reverse trend. The variation of temperature field against temperature slip parameter K_2 is demonstrated in figure 7(a). The temperature distribution show decreasing behavior with higher K_2 . The thermal accommodation coefficient is enhanced on a physical level for larger amount of K_2 , as a result, there is less heat diffusion in the flow direction. As a result, $\theta(\zeta)$ decreases. Figure 7(b) exemplify the influence of concentration jump parameter (K_3)

on nanoparticle concentration $\phi(\zeta)$. The $\phi(\zeta)$ show opposite behavior with the growth of K_3 . The variation of N_t (thermophoresis characteristics) on concentration and temperature distribution is examined in figures 8(a) and (b). The temperature and nanoparticle concentration distribution enhance with N_t . From the physical point of view, it is seen that thermophoretic force warm molecules travel from the hottest fluid area to the coldest fluid region in this type of flow,

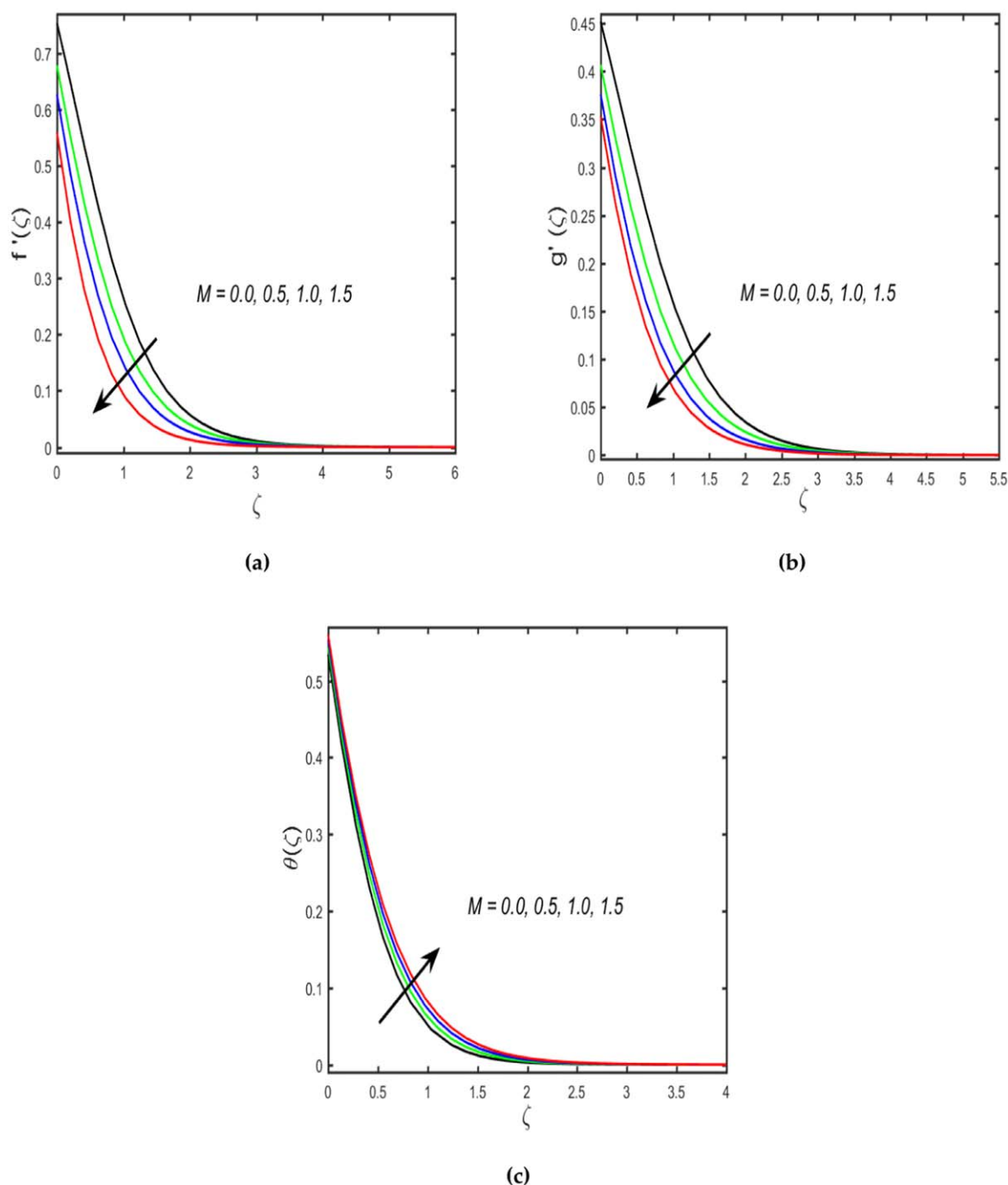
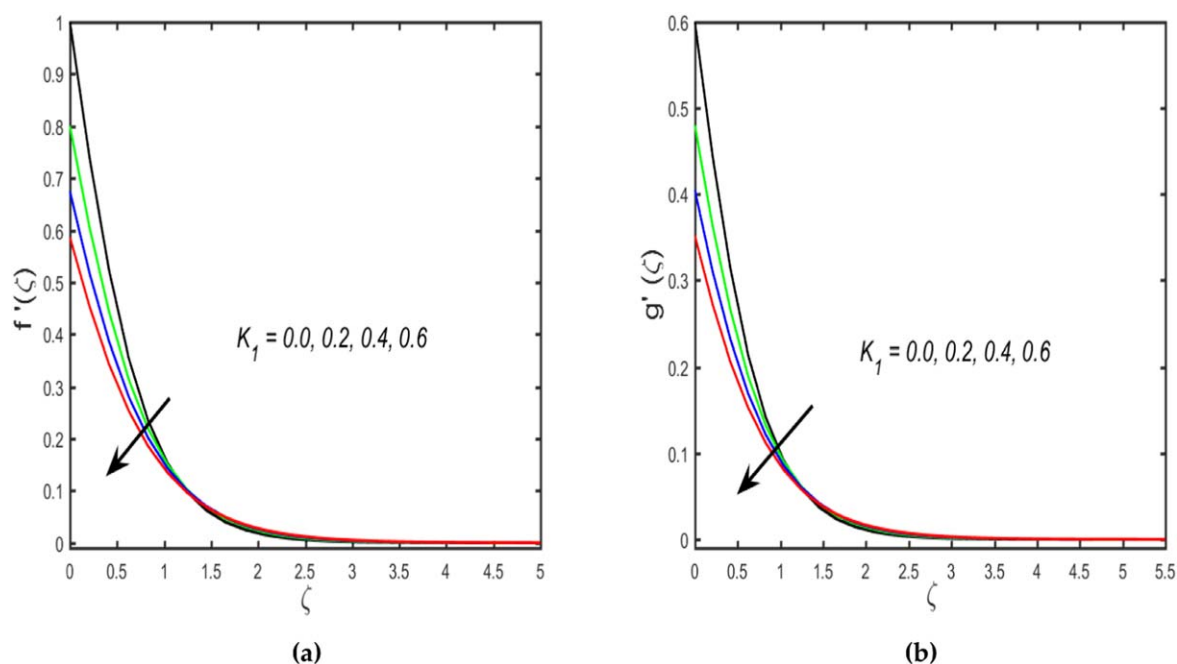
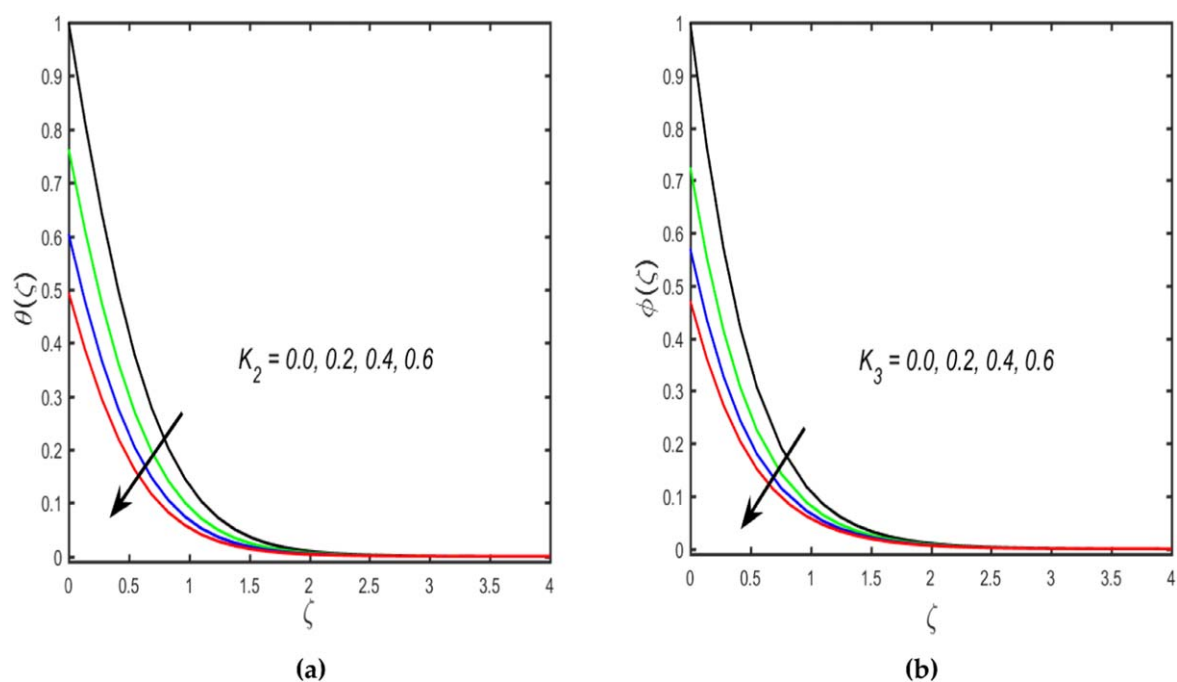


Figure 5. (a)–(c): Plots of M along $f'(\zeta)$, $g'(\zeta)$ and $\theta(\zeta)$.

causing fluid particles to improve temperature and concentration distribution. Further, their corresponding thickness of thermal and concentration boundary layer enhances with N_b .

The effect of the N_b (Brownian motion parameter) on the $\theta(\zeta)$ and $\phi(\zeta)$ plots is seen in figures 9(a) and (b). It is found that by the escalation N_b the temperature field raises, and concentration become lowering. Physically, the collisions between the fluid particles grow as the value of N_b rises. As a result, extra heat is produced, causing the fluid temperature to

rise and the fluid concentration to fall. Figure 10(a) shows the influence of S_c on the nanoparticle concentration. It is deliberated that the concentration sketch reduces by the improvement of S_c . Physically, S_c is a mathematical representation of the relationship between momentum and mass diffusivity. The mass diffusivity is devalued by the increment of the Schmidt number, thereby the mass concentration of decreases. In figure 10(b), the efficiency of temperature ratio characteristics (δ) is observed. It is noticed that mass concentration decaying function for larger δ .

Figure 6. (a), (b): Plot of K_1 along $f'(\zeta)$ and $g'(\zeta)$.Figure 7. (a), (b): Plots of K_2 and K_3 along $\theta(\zeta)$ and $\phi(\zeta)$.

4. Conclusions

The flow model of Maxwell nanomaterial liquid with Joule heating, multiple slips and thermal radiation, is addressed utilizing MATLAB algorithm bvp4c non-Newtonian fluid flow across a stretch sheet affects a wide range of industries and applications of engineering. The petroleum industry, polymeric fluids, solar plants, air conditioning, heat exchangers, refrigeration, food

processing, cooling towers, transpiration, plastic and rubber sheet manufacture, crop damage due to freezing, and chemical engineering are all covered by this fluids model.

The key points of the paper are arranged as follows:

- The thickness of the momentum layer is reduced by the wall thickness parameter, Deborah number, and magnetic parameter. Such that, the fluid velocities are reduced.

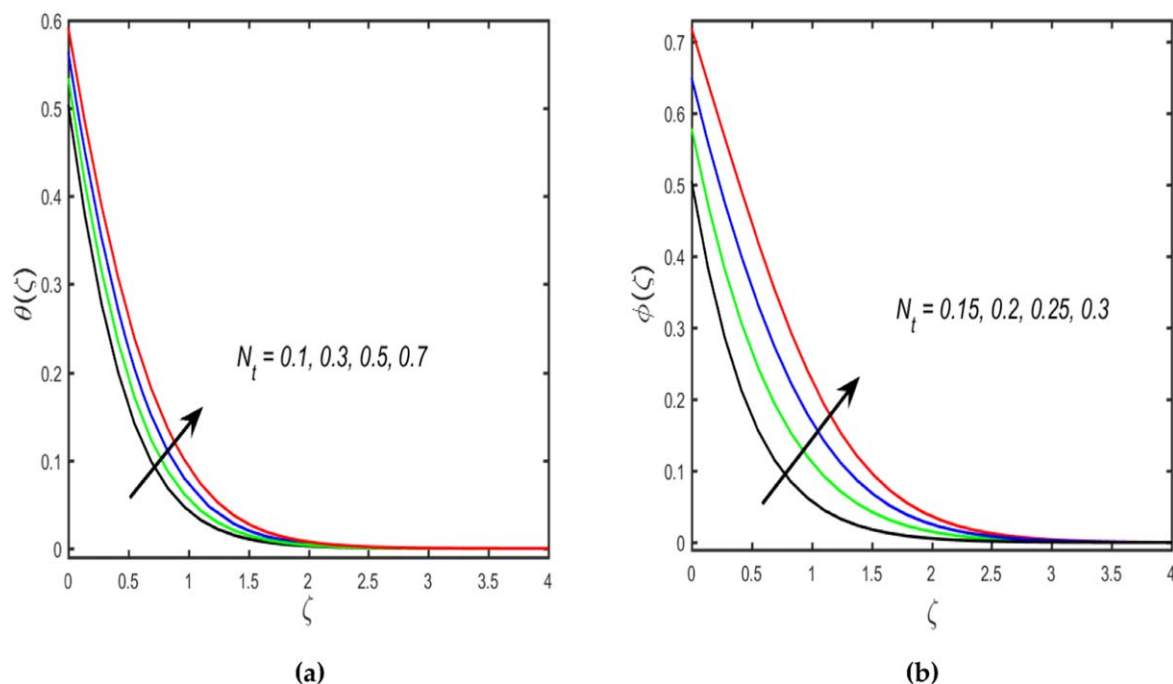


Figure 8. (a), (b): Plot of N_t along $\theta(\zeta)$ and $\phi(\zeta)$.

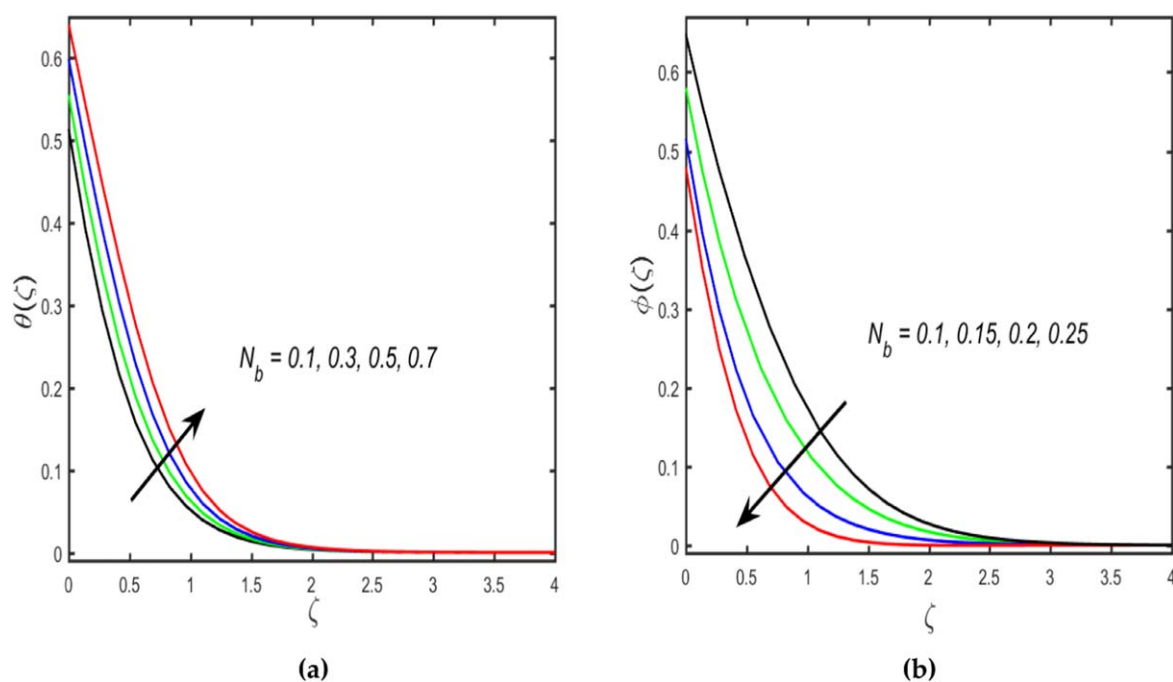


Figure 9. (a), (b): Plot of N_b along $\theta(\zeta)$ and $\phi(\zeta)$.

- The thermal thickness layer boosts with heat generation, radiation, and magnetic parameters, while it reduces for larger amount of thermophoresis, temperature jump and Brownian motion parameter.
- The concentration function is lessened when the Schmidt number, concentration difference parameter, concentration jump parameter, and Brownian motion parameter improve, however it is enhanced as the thermophoresis parameter increases.
- The velocity gradient $f''(0)$ and $g''(0)$ rises by boosting the value of the wall thickness characteristic and power-law index characteristic.
- Characteristic of radiation and power-law index parameter enhance the heat transfer rate, while the heat generation, magnetic characteristic, and temperature jump characteristic reduced the heat transfer rate.
- Schmidt number and Binary chemical reaction characteristics increase the mass transport rate, while the

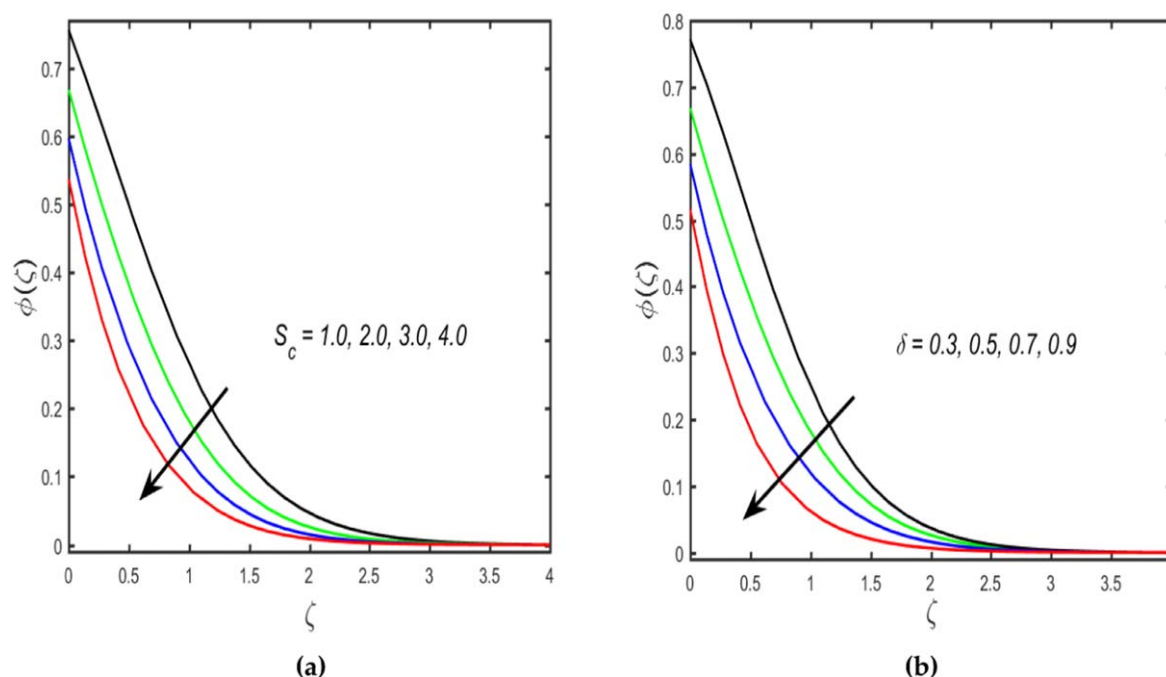


Figure 10. (a), (b): Plots of Sc and δ along $\phi(\zeta)$.

concentration jump parameter decreases the mass transfer rate.

Acknowledgments

The authors extend their appreciation the deanship of Scientific research at King Khalid University for funding through research group program under grant number R.G.P 1/135/42.

References

- [1] Nagendramma V, Raju C S K, Mallikarjuna B, Shehzad S A and Leelarathnam A 2018 3D Casson nanofluid flow over slendering surface in a suspension of gyrotactic microorganisms with Cattaneo–Christov heat flux *Appl. Math. Mech.* **39** 623–38
- [2] Prakash M and Devi S 2016 Hydromagnetic hybrid Al_2O_3 -Cu/water nanofluid flow over a slendering stretching sheet with prescribed surface temperature *Asian J. Res. Soc. Sci. Humanit.* **6** 1921–36
- [3] Hayat T, Qayyum S, Alsaedi A and Ahmad B 2018 Mechanisms of double stratification and magnetic field in flow of third grade fluid over a slendering stretching surface with variable thermal conductivity *Results Phys.* **8** 819–28
- [4] Reddy J R, Sugunamma V and Sandeep N 2018 Thermophoresis and Brownian motion effects on unsteady MHD nanofluid flow over a slendering stretching surface with slip effects *Alexandria Eng. J.* **57** 2465–73
- [5] Gayatri M, Jayaramireddy K and Jayachandra Babu M 2019 Nonlinear convective flow of maxwell fluid over a slendering stretching sheet with heat source/sink *J. Appl. Comput. Mech.* **8** 60–70
- [6] Reddy S R R, Reddy P B A and Bhattacharyya K 2019 Effect of nonlinear thermal radiation on 3D magneto slip flow of Eyring–Powell nanofluid flow over a slendering sheet with binary chemical reaction and Arrhenius activation energy *Adv. Powder Technol.* **30** 3203–13
- [7] Mabood F, Ashwinkumar G P and Sandeep N 2020 Simultaneous results for unsteady flow of MHD hybrid nanoliquid above a flat/slendering surface *J. Therm. Anal. Calorim.* **146** 1–13
- [8] Kumar M, Reddy G J and Dalir N 2018 Transient entropy analysis of the magnetohydrodynamics flow of a Jeffrey fluid past an isothermal vertical flat plate *Pramana* **91** 1–11
- [9] Kumar K A, Sugunamma V and Sandeep N 2020 Influence of viscous dissipation on MHD flow of micropolar fluid over a slendering stretching surface with modified heat flux model *J. Therm. Anal. Calorim.* **139** 3661–74
- [10] Abdelhafez M A, Awad A A, Nafe M A and Eisa D A 2021 Time-dependent viscous flow of higher-order reactive MHD Maxwell nanofluid with Joule heating in a porous regime *Waves Random Complex Medium* **31** 1–21
- [11] Lu D, Ramzan M, Ahmad S, Chung J D and Farooq U 2017 Upshot of binary chemical reaction and activation energy on carbon nanotubes with Cattaneo–Christov heat flux and buoyancy effects *Phys. Fluids* **29** 123103
- [12] Iqbal Z, Khan M, Ahmed A and Nadeem S 2020 Features of thermophoretic and Brownian forces in Burgers fluid flow subject to Joule heating and convective conditions *Phys. Scr.* **96** 015211
- [13] Ali A, Noreen A, Saleem S, Aljohani A F and Awais M 2021 Heat transfer analysis of Cu– Al_2O_3 hybrid nanofluid with heat flux and viscous dissipation *J. Therm. Anal. Calorim.* **143** 2367–77
- [14] Khan, Saeed N, Kumam P and Thounthong P 2021 Magnetic field promoted irreversible process of water based nanocomposites with heat and mass transfer flow *Sci. Rep.* **11** 1–25
- [15] Sheikholeslami M, Rezaeianjouybari B, Darzi M, Shafee A, Li Z and Nguyen T K 2019 Application of nano-refrigerant for boiling heat transfer enhancement employing an experimental study *Int. J. Heat Mass Transfer* **141** 974–80
- [16] Kumar K G 2019 Exploration of flow and heat transfer of non-Newtonian nanofluid over a stretching sheet by considering slip factor *Int. J. Numer. Methods Heat Fluid Flow* **30** 1991–2001

- [17] Ahmad S, Coban H H, Khan M N, Khan U, Shi Q H, Muhammad T and Kadry S 2021 Computational analysis of the unsteady 3D chemically reacting MHD flow with the properties of temperature dependent transverse suspended Maxwell nanofluid *Case Stud. Therm. Eng.* **26** 101169
- [18] Kumar K G, Khan M N, Osman M, Alharbi A R, Rahimi-Gorji M and Alarifi I M 2019 Slip flow over a non-Newtonian fluid through a Darcy–Forchheimer medium: numerical approach *Mod. Phys. Lett. B* **33** 1950448
- [19] Malik R, Khan M, Shafiq A, Mushtaq M and Hussain M 2017 An analysis of Cattaneo–Christov double-diffusion model for Sisko fluid flow with velocity slip *Results Phys.* **7** 1232–7
- [20] Ahmad S, Nadeem S and Muhammad N 2019 Boundary layer flow over a curved surface imbedded in porous medium *Commun. Theor. Phys.* **71** 344
- [21] Awais M, Raja M A Z, Awan S E, Shoaib M and Ali H M 2021 Heat and mass transfer phenomenon for the dynamics of Casson fluid through porous medium over shrinking wall subject to Lorentz force and heat source/sink *Alexandria Eng. J.* **60** 1355–63
- [22] Bouvier P, Stouffs P and Bardon J P 2005 Experimental study of heat transfer in oscillating flow *Int. J. Heat Mass Transfer* **48** 2473–82
- [23] Punith Gowda R J, Naveen Kumar R, Jyothi A M, Prasannakumara B C and Sarris I E 2021 Impact of binary chemical reaction and activation energy on heat and mass transfer of marangoni driven boundary layer flow of a non-Newtonian nanofluid *Processes* **9** 702
- [24] Jarny Y 2001 Determination of heat sources and heat transfer coefficient for two-dimensional heat flow—numerical and experimental study *Int. J. Heat Mass Transfer* **44** 1309–22
- [25] Reddy M G, Sudharani M V V N L and Kumar K G 2020 An analysis of dusty slip flow through a single-/multi-wall carbon nanotube *Contin. Mech. Thermodyn.* **32** 971–85
- [26] Choi T J, Park M S, Kim S H and Jang S P 2021 Experimental study on the effect of nanoparticle migration on the convective heat transfer coefficient of EG/water-based Al_2O_3 nanofluids *Int. J. Heat Mass Transfer* **169** 120903
- [27] Zhang X and Zhang Y 2021 Experimental study on enhanced heat transfer and flow performance of magnetic nanofluids under alternating magnetic field *Int. J. Therm. Sci.* **164** 106897
- [28] Reddy M G, Rani M S, Kumar K G, Prasannakumar B C and Chamkha A J 2020 Cattaneo–Christov heat flux model on Blasius–Rayleigh–Stokes flow through a transitive magnetic field and Joule heating *Physica A* **548** 123991
- [29] Navier C L M H 1823 Mémoire sur les lois du mouvement des fluides *Mémoires de l'Académie Royale des Sciences de l'Institut de France* **6** 389–440
- [30] Maxwell J C 1879 On stresses in rarified gases arising from inequalities of temperature *Phil. Trans. R. Soc.* **170** 231–56
- [31] Andersson H I 2002 Slip flow past a stretching surface *Acta Mech.* **158** 121–5
- [32] Nawaz M, Rafiq S, Qureshi I H and Saleem S 2020 Combined effects of partial slip and variable diffusion coefficient on mass and heat transfer subjected to chemical reaction *Phys. Scr.* **95** 035222
- [33] Archana M, Praveena M M, Kumar K G, Shehzad S A and Ahmad M 2020 Unsteady squeezed Casson nanofluid flow by considering the slip condition and time-dependent magnetic field *Heat Transfer* **49** 4907–22
- [34] Imran M A, Riaz M B, Shah N A and Zafar A A 2018 Boundary layer flow of MHD generalized Maxwell fluid over an exponentially accelerated infinite vertical surface with slip and Newtonian heating at the boundary *Results Phys.* **8** 1061–7
- [35] Aziz A and Shams M 2020 Entropy generation in MHD Maxwell nanofluid flow with variable thermal conductivity, thermal radiation, slip conditions, and heat source *AIP Adv.* **10** 015038
- [36] Souayeh B, Kumar K G, Reddy M G, Rani S, Hdhiri N, Alfannakh H and Rahimi-Gorji M 2019 Slip flow and radiative heat transfer behavior of Titanium alloy and ferromagnetic nanoparticles along with suspension of dusty fluid *J. Mol. Liq.* **290** 111223
- [37] Ahmad S, Nadeem S, Muhammad N and Khan M N 2021 Cattaneo–Christov heat flux model for stagnation point flow of micropolar nanofluid toward a nonlinear stretching surface with slip effects *J. Therm. Anal. Calorimetry* **143** 1187–99
- [38] Khan M I and Alzahrani F 2021 Nonlinear dissipative slip flow of Jeffrey nanomaterial towards a curved surface with entropy generation and activation energy *Math. Comput. Simul.* **185** 47–61
- [39] Ahmad S and Nadeem S 2020 Analysis of activation energy and its impact on hybrid nanofluid in the presence of Hall and ion slip currents *Appl. Nanosci.* **10** 5315–30
- [40] Nandi S, Kumbhakar B, Seth G S and Chamkha A J 2021 Features of 3D magneto-convective nonlinear radiative Williamson nanofluid flow with activation energy, multiple slips and Hall effect *Phys. Scr.* **96** 065206
- [41] Kumar K G, Krishnamurthy M R and Rudraswamy N G 2019 Boundary layer flow and melting heat transfer of Prandtl fluid over a stretching surface by considering Joule heating effect *Multidiscipline Model. Mater. Struct.* **15** 337–52
- [42] Khan M N, Nadeem S, Ahmad S and Saleem A 2020 Mathematical analysis of heat and mass transfer in a Maxwell fluid *Proc. Inst. Mech. Eng. C* **235** 0954406220976704
- [43] Swain K, Sampada K P and Dash G C 2018 Effects of non-uniform heat source/sink and viscous dissipation on MHD boundary layer flow of Williamson nanofluid through porous medium *Defect and Diffusion Forum* vol 389 (Bäch: Trans Tech Publications Ltd) pp 110–27
- [44] Suraiah Palaiah S, Basha H, Reddy G J and Sheremet M A 2021 Magnetized dissipative sores effect on chemically reactive Maxwell fluid over a stretching sheet with joule heating *Coatings* **11** 528
- [45] Ahmed A, Khan M, Sarfraz M, Ahmed J and Iqbal Z 2021 Forced convection in 3D Maxwell nanofluid flow via Cattaneo–Christov theory with Joule heating *Proc. Inst. Mech. Eng. E* **235** 0954408921999633
- [46] Islam S, Khan A, Kumam P, Alrabaiah H, Shah Z, Khan W and Jawad M 2020 Radiative mixed convection flow of maxwell nanofluid over a stretching cylinder with joule heating and heat source/sink effects *Sci. Rep.* **10** 1–18